



NONLINEAR RESPONSE OF THE MASS-SPRING MODEL WITH NONSMOOTH STIFFNESS

GRZEGORZ LITAK

*Department of Applied Mechanics, Lublin University of Technology,
Nadbystrzycka 36, PL-20-618 Lublin, Poland*

*Dipartimento di Architettura, Costruzioni e Strutture,
Università Politecnica delle Marche,
Via Breccie Bianche 60131 Ancona, Italy*

JESÚS M. SEOANE, SAMUEL ZAMBRANO and MIGUEL A. F. SANJUÁN*

*Nonlinear Dynamics, Chaos and Complex Systems Group,
Departamento de Física, Universidad Rey Juan Carlos,
Tulipán s/n, 28933 Móstoles, Madrid, Spain*

**Department of Mathematics, School of Science,
Beijing Jiaotong University, Beijing 100044, P. R. China*

Received October 20, 2010

In this paper, we study the nonlinear response of the nonlinear mass-spring model with non-smooth stiffness. For this purpose, we take as prototype model, a system that consists of the double-well smooth potential with an additional spring component acting on the system only for large enough displacement. We focus our study on the analysis of the homoclinic orbits for such nonlinear potential for which we observe the appearance of chaotic motion in the presence of damping effects and an external harmonic force, analyzing the crucial role of the linear spring in the dynamics of our system. The results are shown by using both the Melnikov analysis and numerical simulations. We expect our work to have implications on problems concerning the suspension of vehicles, among others.

Keywords: Nonlinear oscillations; Melnikov criterion; chaos; nonsmooth dynamical systems.

1. Introduction

There is a rich bibliography on chaotic systems which are defined by a set of ordinary differential equations including nonlinear but with smooth functions of displacement or velocity [Sprott, 2003]. Nonsmooth systems are very common in engineering [Leine *et al.*, 2000; Wiercigroch & de Kraker, 2000; Radons & Neugebauer, 2004; Litak *et al.*, 2007; Pavlovskaja & Wiercigroch, 2007] where they have relevant implications. In the present paper, we examine the dynamics of the two-stage mass-spring oscillator as shown in Fig. 1.

In this system, the two considered springs are connected in a parallel way. One of them is the nonlinear characteristics that produces the double-well Duffing potential while the other acts according to Hooke's law, $F = -kx$, as shown in Fig. 1. Such connections of springs are often considered in practical situations as in the suspension of vehicles [Verros *et al.*, 2000; Von Wagner, 2004], among others. The main goal of our paper is to analyze the effect of the linear spring on the two exterior nonlinear springs. We focus our attention on the physical situations in which chaotic or periodic behavior

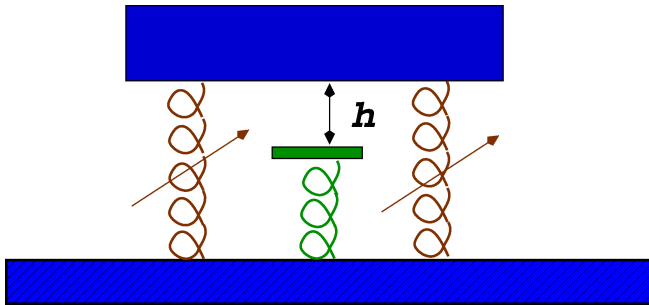


Fig. 1. Schematic plot of the two-stage spring-mass model. The effective exterior springs in the figure are assumed to have nonlinear characteristics, while the interior, which introduces nonsmoothness, has linear characteristics. h denotes the tip position of the spring-free length with respect to the equilibrium point $x = 0$.

takes place, depending on the value of the different parameters of the system. The study of the bifurcation diagrams and the basins of attraction elucidate the existence of new attractors into the system and we add the effect of the asymmetric term. Furthermore, they enlighten the bifurcations by which such attractors arise.

This paper is organized as follows. Section 2 presents a description of our model. In Sec. 3, we solve the corresponding differential equations and discuss the results. We use the Melnikov criterion [Melnikov, 1963; Guckenheimer & Holmes, 1983] to predict the existence of periodic solution. The critical force-to-damping ratio is confirmed by the numerical simulations. As the examined system is a nonsmooth example, one has to modify the Melnikov formula by adding the extra terms related to the singular points of nonsmoothness [Kunze & Küpper, 2001] (at these points, the functions do not fulfill the C^1 class requirements). On the other hand, the numerical estimation of the integral can be done. This concept, used in previous works [Litak *et al.*, 2008], is used in Sec. 4. After presenting the numerical results, confirming the estimated critical parameters, the paper ends with conclusions and the final remarks are presented in Sec. 5.

2. Model Description

The model we take as prototype, according to Fig. 1, is given by the nondimensional equation of motion:

$$\begin{aligned} \ddot{x} + \alpha\dot{x} - ax + bx^3 + k(x-h)\Theta(x-h) \\ = F \sin(\omega t), \end{aligned} \quad (1)$$

where α is the damping parameter, a and b are linear and cubic parts of the nonlinear spring and k is a linear spring of defined length and a nonsymmetrical contact loss. $\Theta(x)$ is the Heaviside step function, F is the amplitude of a harmonic excitation and h is the position of the tip of the spring-free length with respect to the equilibrium point $x = 0$. We observe that if $k = 0$, we have the well known Duffing oscillator [Duffing, 1918; Aguirre & Sanjuán, 2002; Baltanás *et al.*, 2001], that is, the double-well potential.

The restoring force $F(x)$ is defined by the potential $V(x)$ (Fig. 2) as follows

$$\begin{aligned} F(x) &= -\frac{\partial V}{\partial x} \\ &= ax - bx^3 - k(x-h)\Theta(x-h), \end{aligned} \quad (2)$$

$$V(x) = -\frac{ax^2}{2} + \frac{bx^4}{4} + \frac{k(x-h)^2\Theta(x-h)}{2}, \quad (3)$$

where we have taken $x_0 + h' = h$ with $x_0 = 1$ and $h' = -0.1$. From now on and without loss of generality, we fix $a = 1$ and $b = 1$.

Figure 2 shows a profile of the potential in both cases, the Duffing oscillator and the Duffing oscillator with a linear spring. We clearly observe the asymmetry (denoted by the dotted curve on the right-hand side of the figure) produced by the linear restoring force. Notice that the solid red curve represents the symmetric double well potential.

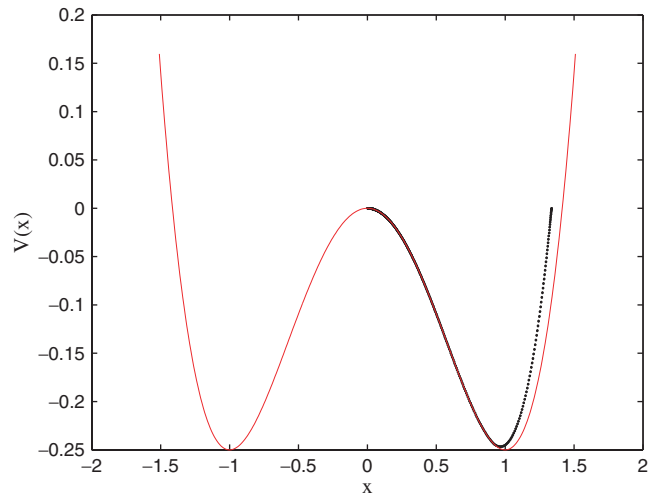


Fig. 2. Solid curve represents the Duffing symmetric potential $V_1(x) = -\frac{x^2}{2} + \frac{x^4}{4}$ and the present potential with an additional spring $V(x) = -\frac{x^2}{2} + \frac{x^4}{4} + k\frac{(x-x_0-h')^2\Theta(x-x_0-h')}{2}$, for $k = 1$, is represented by the dotted curve. The parameter is $x_0 + h' = h$, $x_0 = 1$ is the position of the right-hand side stable equilibrium point, while $h' = -0.1$ denotes the tip position of the spring-free length.

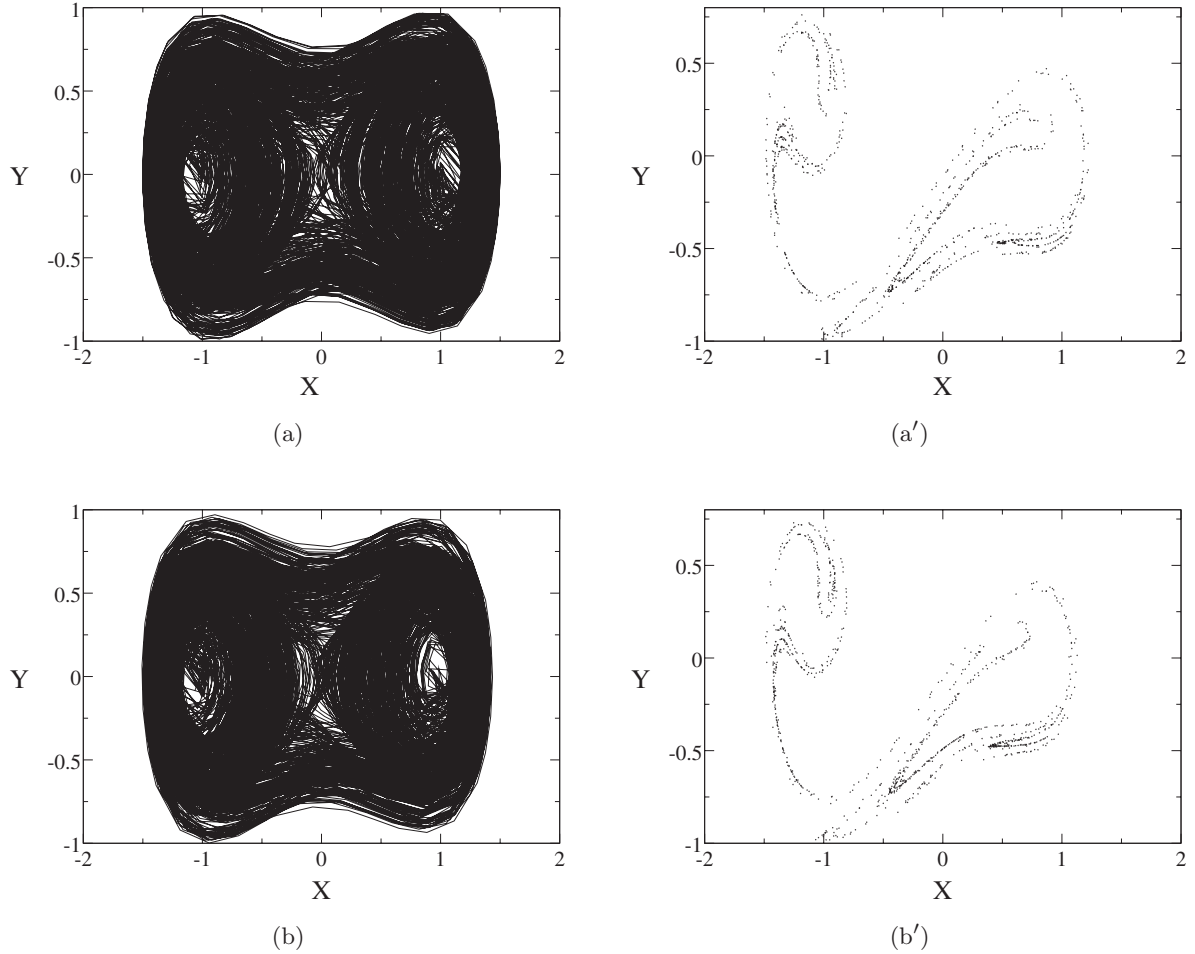


Fig. 3. Numerical plots of both (a) and (b) trajectories and (a') and (b') Poincaré sections, for the Duffing oscillator case and for the nonsmooth case with parameter values $\alpha = 0.15$, $F = 0.258$, $k = 0.2$ and $h = 0.3$, respectively. We observe the effect of the nonsmooth term on the right-hand side of the images: in the presence of nonsmoothness, both the trajectories and the attractor look similar to the unperturbed ones, but their right-hand side is slightly compressed.

In order to understand better the behavior of our system, we show numerical plots of both, trajectories in phase space and Poincaré sections. For this purpose, we have taken the following values of the parameters: $\alpha = 0.15$, $\omega = 1$ and $F = 0.258$. Figures 3(a) and 3(a') represent both the typical chaotic trajectory and the typical Poincaré section of the Duffing oscillator for the smooth case. Furthermore, we can see in Fig. 4, the bifurcation diagram of the x variable as a function of the forcing amplitude F , and we can see that $F = 0.258$ is well into the chaotic region.

Figures 3(b) and 3(b') show the same kind of plots for the nonsmooth case for $k = 0.2$ and $h = 0.3$. We observe, on the right-hand side (region in which $x > 0$) of Figs. 3(a') and 3(b'), the effect of the nonsmooth term. Provided that the profile of the right well of the Duffing oscillator becomes

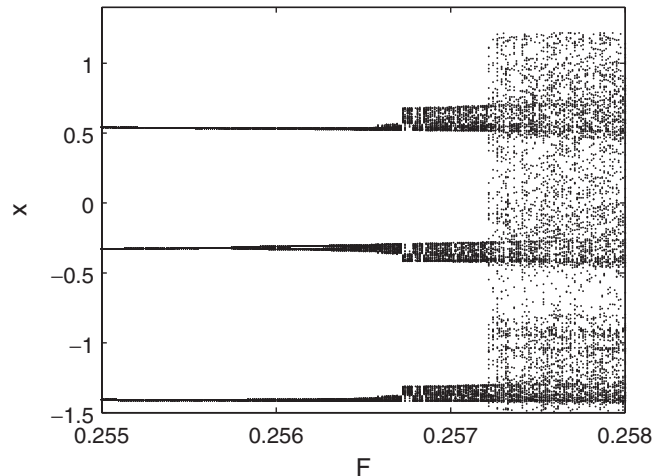


Fig. 4. Numerical bifurcation diagram of the Duffing oscillator in the absence of the linear spring ($\alpha = 0.15$). We observe periodic regions and chaotic regions depending on the value of F . The onset of chaos takes place at $F \simeq 0.257$.

steeper due to the nonsmooth term, we see how both the right-hand side of the trajectories and the attractor are slightly compressed compared to the unperturbed case (Fig. 2).

In the next section we provide, by using Melnikov analysis, theoretical arguments in order to show the different regions of parameters in which the system is in a chaotic regime or in a periodic regime.

3. Melnikov Analysis

In this section, we use Melnikov analysis [Moon & Li, 1985; Baltanás *et al.*, 2002; Almendral *et al.*, 2004] in order to provide analytical arguments of the different dynamical behaviors of our system.

According to the Melnikov analysis, we assume that the force and damping parameter can be treated as perturbations, so that we can rewrite:

$$F \rightarrow \epsilon \tilde{F}, \quad \alpha \rightarrow \epsilon \tilde{\alpha}. \quad (4)$$

For our convenience and without any loss of generality in the results, we choose $a = b = k = 1$, for which the equations of the system can be rewritten as follows:

$$\dot{x} = v, \quad (5)$$

$$\begin{aligned} \dot{v} &= x - x^3 - (x - h)\Theta(x - h) \\ &= \epsilon(-\tilde{\alpha}\dot{x} + \tilde{F} \sin(\omega t)). \end{aligned} \quad (6)$$

Thus, the unperturbed Hamiltonian, i.e. in the absence of both forcing and damping, reads as

$$H_0 = \frac{v^2}{2} - \frac{x^2}{2} + \frac{x^4}{4} + k \frac{(x - h)^2 \Theta(x - h)}{2}. \quad (7)$$

Looking for the homoclinic orbits in the Melnikov approach, we obtain the left- (for $x \leq 0$) and right- (for $x \geq 0$) hand side loops connecting the saddle point $x = 0$ and $H_0|_{x=0} = 0$ by integrating the following expression:

$$\frac{dt}{dx} = \frac{1}{v} = \frac{1}{\sqrt{2V(x)}}. \quad (8)$$

Consequently, the integration of the equation above leads to

$$t - t_0 = \frac{1}{\sqrt{x^2 - \frac{x^4}{2} - k(x - h)^2 \Theta(x - h)}}. \quad (9)$$

In the case of the typical double-well potential and for the right-hand side half-plane $x < 0$, we can

easily integrate the above expression to the analytic formula:

$$\begin{aligned} x^*(t) &= \pm \frac{\sqrt{2}}{\cosh(t - t_0)}, \\ v^*(t) &= \pm \frac{\sqrt{2} \tanh(t - t_0)}{\cosh(t - t_0)}. \end{aligned} \quad (10)$$

After adding perturbations, the homoclinic orbits split into the so-called stable and unstable manifolds, denoted by W_S and W_U , respectively. The existence of cross-sections between W_S and W_U manifolds signals Smale's horseshoe scenario of transition to chaos (see Fig. 7). Consequently, the distance d between the invariant manifolds can be estimated in terms of the Melnikov function since $d \sim M(t_0)$:

$$M(t_0) = \int_{-\infty}^{\infty} h_0(x^*, v^*) \wedge h_1(x^*, v^*) dt, \quad (11)$$

where \wedge defines the wedge product ($dx \wedge dv = -dx \wedge dv$, $dx \wedge dx = dv \wedge dv = 0$). The corresponding differential forms h_0 mean the gradient of the unperturbed Hamiltonian

$$\begin{aligned} h_0 &= (-x^* + (x^*)^3 + (x - h)\Theta(x^* - h))dx \\ &\quad + v^* dv, \end{aligned} \quad (12)$$

while h_1 is a perturbation to the same Hamiltonian

$$h_1 = (\tilde{F} \sin(\omega t) - \tilde{\alpha} v^*) dx. \quad (13)$$

It is important that all differential forms in the above expressions are defined on the homoclinic orbits $(x, v) = (x^*, v^*)$. Thus the Melnikov function $M(t_0)$ reads:

$$M(t_0) = \int_{-\infty}^{\infty} v^* (\tilde{F} \sin(\omega t) - \tilde{\alpha} v^*) dt. \quad (14)$$

Thus a condition for a global homoclinic transition, corresponding to a horseshoe type, can be written as:

$$\bigvee_{t_0} M(t_0) = 0 \quad \text{and} \quad \frac{\partial M(t_0)}{\partial t_0} \neq 0. \quad (15)$$

The above condition is valid [Guckenheimer & Holmes, 1983] for smooth potential belonging to C^2 class ($V \in C^2$).

On the other hand, the nonsmooth case for $k \neq 0$ (Figs. 5 and 6) is difficult for analytic treatment but the corresponding Melnikov criterion [Eqs. (11)–(15)] could be found numerically. Note

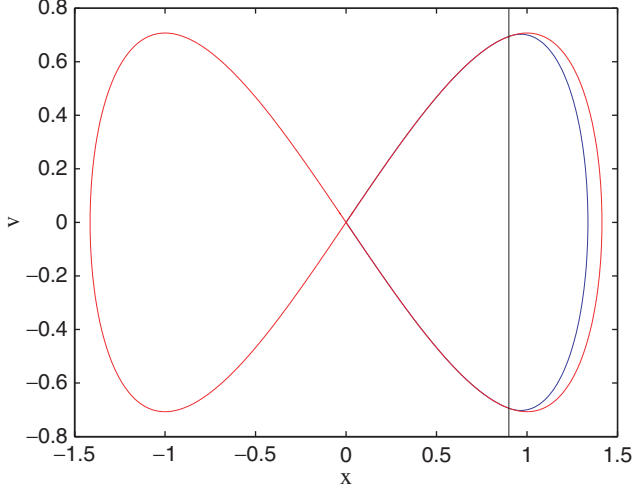


Fig. 5. The homoclinic orbit: (red) Duffing symmetric potential $V_1(a) = -\frac{x}{2} + \frac{x^4}{4}$, (blue) the right-hand side homoclinic orbit for the potential with an additional spring. The vertical line shows the switching point of the additional spring potential $x = h = x_0 + h'$ ($x_0 = 1$, $h' = -0.1$), and $k = 1$.

that in this situation the potential is not smooth enough as it belongs to C^1 class functions. Thus according to Kunze and Küpper [2001] there would be corrections related to the singular points of non-smoothness $x = h$. However, the above corrections are more important for analytical and precise estimation of a homoclinic bifurcation. In our case, we solve the integral numerically, and our approximation will include Kunze and Küpper [2001] corrections within the integration error. It should be noted that corrections are given, in some sense, by averaging the integral kernel in different limits $x \rightarrow h$.

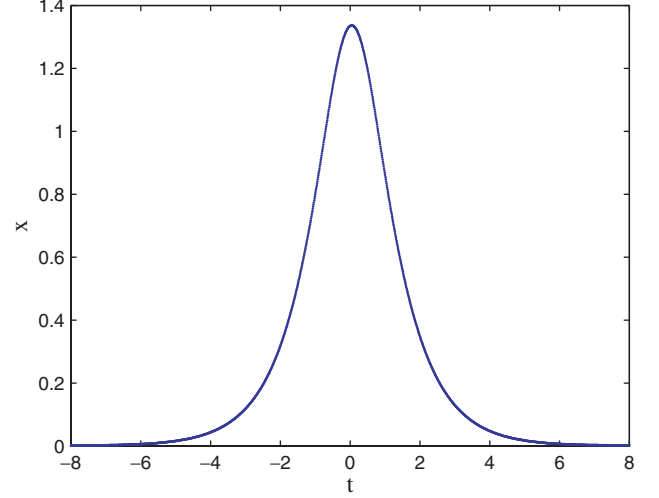
Finally, from Eqs. (14) and (15), the critical region of the ratio $\eta = \tilde{F}/\tilde{\alpha} = F/\alpha$ as a function of ω can be estimated as

$$\eta(\omega) = \min \left| \frac{I_1}{I_2(\omega)} \right|, \quad (16)$$

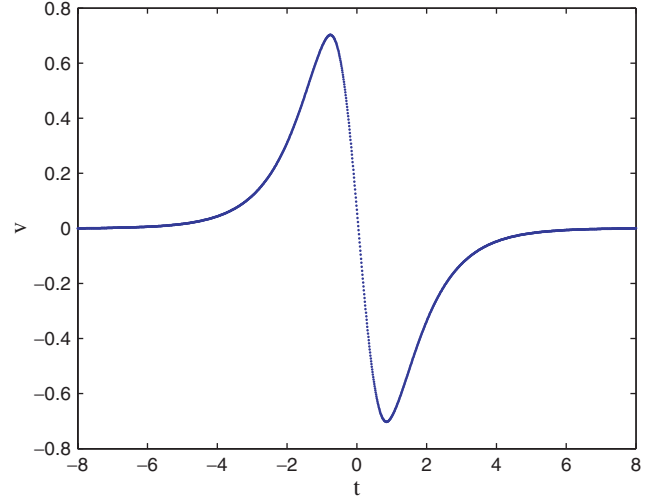
where integrals I_1 and I_2 have the following forms

$$\begin{aligned} I_1 &= \int_{-\infty}^{\infty} (v^*(t))^2 dt \quad \text{and} \\ I_2 &= \int_{-\infty}^{\infty} v^*(t) \sin(\omega t + \omega t_0) dt. \end{aligned} \quad (17)$$

The condition for the second potential well on the left-hand side in Fig. 2 with a smooth heteroclinic orbit (Fig. 5) can be expressed analytically as for the case $k = 0$. Introducing $v^*(t)$ to Eq. (17) [Holmes, 1979; Guckenheimer & Holmes, 1983] we



(a)



(b)

Fig. 6. (a) Displacement and (b) velocity for the numerically obtained right-hand side homoclinic loop for the potential with additional spring ($V = -\frac{x^2}{2} + \frac{x^4}{4} + k\frac{(x-h)^2\Theta(x-h)}{2}$, with $k = 1$, $h = 0.9$).

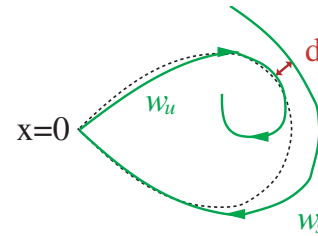


Fig. 7. A schematic picture of unperturbed (plotted with a dotted line) and perturbed homoclinic orbits (stable W_S and unstable W_U manifolds plotted with full lines). d is the distance between W_s and W_u . $x = 0$ indicates the location of the saddle point.

integrate:

$$I_1 = \frac{4}{3}, \quad I_2 = \frac{\sqrt{2}\pi\omega}{\cosh\left(\frac{\pi\omega}{2}\right)} \sin(\omega t_0), \quad (18)$$

and we choose the free integration parameter t_0 in such a way that $\max|\sin(\omega t_0)| = 1$.

Finally, for the condition on the left-hand side of the potential well (Fig. 2), $\eta(\omega)$ [Eq. (16)] could be expressed analytically as

$$\eta(\omega) = \frac{2\sqrt{2}}{3\pi\omega} \cosh\left(\frac{\pi\omega}{2}\right). \quad (19)$$

The condition for the right-hand side potential well (nonsmooth case) in Fig. 2 (for $k > 0$, $h < 1.4$) has been calculated numerically. By changing h we could see the effect of an additional spring on the dynamics (Fig. 1). The results of the Melnikov analysis are presented in Fig. 8.

Here, we see that the critical separation lines F/α versus ω are placed in nonmonotonic order. The main difference can be observed in the limit of larger ω . For fairly small h [$h = 0.3$, Fig. 5, line (a)] the chaotic region is effectively shrunk while for the medium size h [$h = 0.9$, Fig. 5, line (c)] the chaotic region is extended. These results can be compared to the large h limit [Fig. 5, line (d)] which simultaneously represent the initial Duffing potential without the influence of the additional asymmetric spring (for $k = 0$), or the condition for the second potential

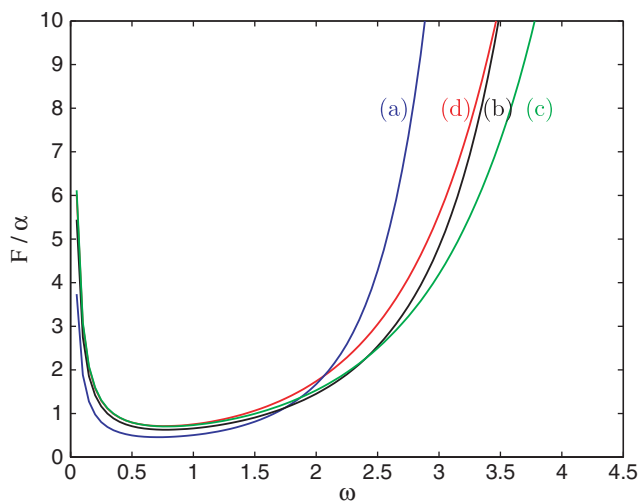


Fig. 8. The critical curves $\eta = F/\alpha$ versus ω that separate the regular (below the curves) and chaotic (above the curves) parameter regions for $k = 1$. Lines (a)–(d) correspond to different values of h , that is, $h = 0.3, 0.6, 0.9$, and $h = 1.6$, respectively.

well on the left-hand side in Fig. 2. As our potential possesses two wells, the transition to chaos would be strongly dependent on the initial conditions. For the initial system state on the right-hand side of the potential well (Fig. 2) the Melnikov criterion would be dependent on h (Fig. 8), while for the system with initial residence in the left potential well the analytic formula Eq. (19) would apply.

Finally, we should note that the Melnikov criterion does not guarantee the steady state chaos appearance, but only the fractalization of the boundaries of the corresponding basins of attraction for different solutions which could result in time series as a transient chaotic motion.

In the next section, we will show numerical simulations to clarify the situation of the asymmetric nonsmooth potential (for different $k > 0$ and h) by means of the corresponding basins of attraction and bifurcation diagrams.

4. Numerical Simulations

In this section, we provide numerical evidence on the results shown previously. For this purpose, we have solved the examined set of equations by using the fourth-order Runge–Kutta integration scheme [Burden & Faires, 1997]. Trajectories in phase space and their corresponding Poincaré sections resulting from these calculations are presented in Fig. 9. One can easily see the difference between the chaotic and regular solutions. Figures 9(a) and 9(a') show a chaotic trajectory for $h = 1$ and $k = 0.2$. If we increase the value of k , say $k = 0.7$, the influence of the linear spring becomes crucial since the chaotic motion disappears and it becomes periodic falling into an attractor, as shown in Fig. 9(b'). It seems then that there is a critical value of k for which a periodic attractor close to the right-hand well of the system appears, making the orbits periodic.

Figures 10(a) and 10(b) provide a deeper insight on this phenomenon. In Fig. 10(a), a bifurcation diagram of the system of x versus F with nonsmooth parameters $k = 0.45$ and $h = 1$ is shown, we can see that for small forcing the system displays periodic behavior, provided that the linear spring is a linear system and it induces regular behaviors into the system. But as F is increased chaos arises in what seems to be an inverse saddle-node bifurcation. Saddle-node bifurcations are widespread in dynamical systems, for example, it is the bifurcation that gives rise to the period-three window in the logistic map [Robinson, 2004]. Figure 10(b) shows

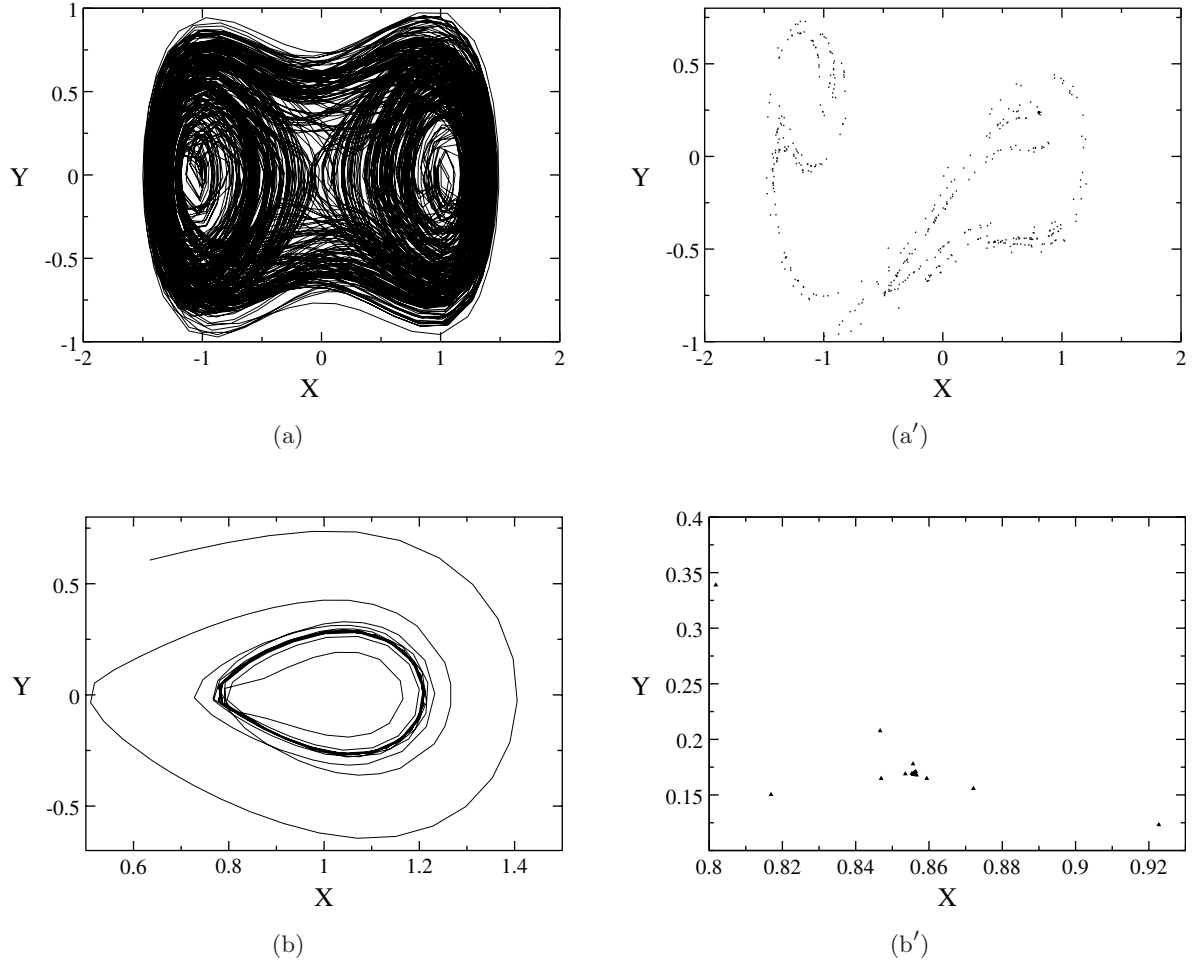


Fig. 9. Numerical plots of both (a) and (b) trajectories and (a') and (b') Poincaré sections, for the nonsmooth case with parameter values (a) and (a') $k = 0.2$ and $h = 1$, and for (b) and (b') $k = 0.7$ and $h = 1$, respectively. We clearly observe the strong effect of the linear spring (b) and (b') in which the motion becomes periodic.

the bifurcation diagram of the variable x versus k for $h = 1$ and $F = 0.258$. We see that the system is chaotic until the value of k is too large and a periodic attractor arises in the right well, so the pre-existing chaotic attractor disappears through a saddle-node bifurcation. An energetic interpretation can be provided for this phenomenon: when adding the nonsmooth stiffness, the system does not change drastically its behavior until k is sufficiently large, when an attractor arises, it stabilizes the orbit. After this, the system can be driven again to the chaotic state by increasing the forcing amplitude F .

The bifurcation diagrams of x versus ω shown in Figs. 10(c) and 10(d) for $k = 0$ and $k = 1$ and $h = 1$, respectively, somehow support the previous considerations. We see that when the system has a nonsmooth stiffness, the system behaves periodically in a range of ω where there is chaos for

$k = 0$. However, as ω is increased (i.e. the frequency of the forcing gets sufficiently large) the system becomes chaotic and it behaves in a way qualitatively very similar to its behavior for $k = 0$, and this holds as ω is increased. The transitions from periodicity to chaos as ω is increased, seems to occur again through an inverse saddle-node bifurcation, similarly to what we observed by fixing k and increasing F . These two situations share then a particular behavior: if the periodic forcing is sufficiently strong (either by increasing F or ω) the influence of the nonsmooth stiffness becomes negligible.

In order to have a better understanding of these results we have plotted the basins of attraction in different situations. Figure 12(a) represents, for $\alpha = 0.15$, $\omega = 1$, $h = 1$ and $F = 0.258$, the typical basin of attraction of the Duffing system [Aguirre & Sanjuán, 2002; Aguirre *et al.*, 2009] without the presence of the linear spring. We observe in green

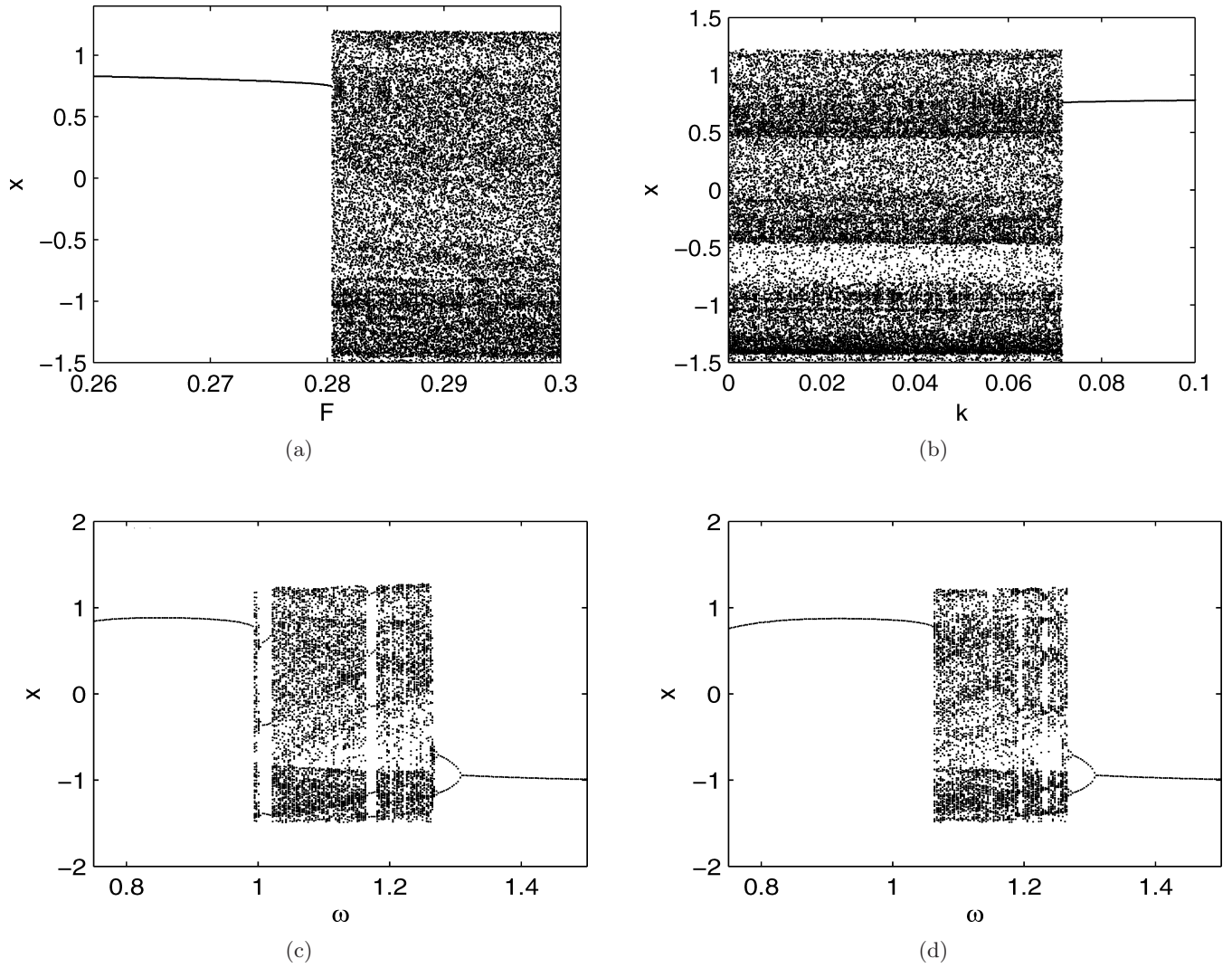


Fig. 10. Numerical bifurcation diagrams of the variable (a) x versus F for $k = 0.45$ and $h = 1$, (b) x versus k for $F = 0.258$, (c) x versus ω for $k = 0$ and $h = 0$ and (d) x versus ω for $k = 1$ and $h = 1$.

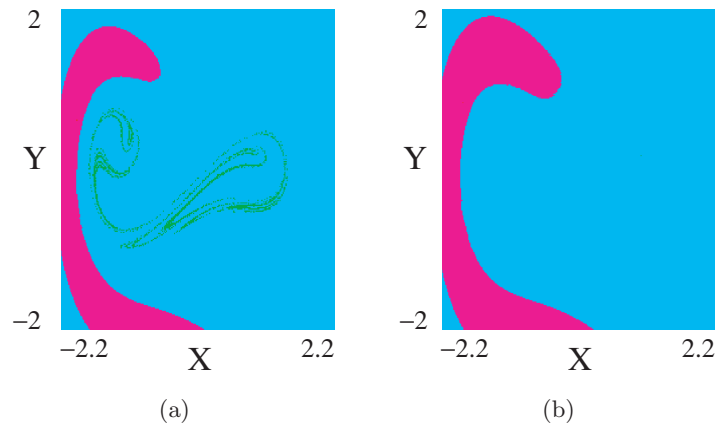


Fig. 11. Plots of the basins of attraction of our system for parameter values: $F = 0.258$, $\alpha = 0.15$, $\omega = 1$ and $h = 1$; (a) corresponds with the Duffing oscillator without the linear spring, (b) represents the case in which $k = 1$. Notice that the strange attractor plotted in green colour is destroyed and the dynamics of the system becomes regular.

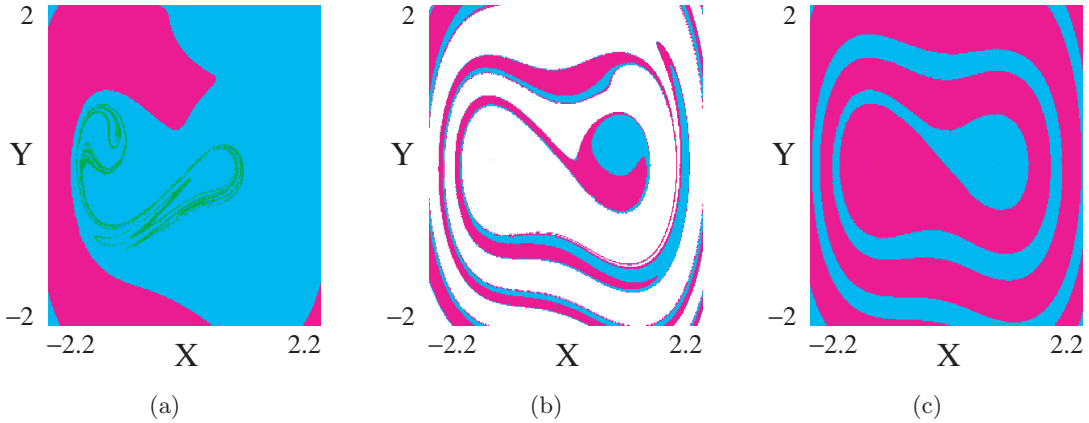


Fig. 12. Plots of the basins of attraction of our system for $F = 0.258$, $F = 0.22$ and $F = 0.15$, respectively. Other parameter values are: $\omega = 1$, $k = 1$, $\alpha = 0.15$ and $h = 0.3$; (a) represents the case in which $\eta = \frac{F}{\alpha} = 1.72$ which corresponds to the chaotic regime as shown in Fig. 8, (b) corresponds to the situation in which $\eta = 0.8$ and therefore the transition between chaotic and periodic motions, as we suggest in Fig. 8. White color denotes the basin of attraction of the new periodic attractor. Finally, the last figure represents the case in which the basins become smooth and the dynamics is completely regular.

color the typical strange attractor of this system. If we add the effect of the nonsmooth term, a complete erosion of the basins takes place as we suggested in Sec. 3. It should be also noted that the Melnikov criterion indicate rather the appearance of the basin boundary destruction. This effect is visible in Fig. 12 where we show the basins of attraction for three values in the vicinity of critical conditions that corroborate the results presented in Fig. 8. Figure 12(a) represents the case $\eta = \frac{F}{\alpha} = 1.72$ which corresponds to the chaotic regime shown in Fig. 8. The green curve shows the chaotic attractor in phase space. Insofar we decrease the value of η , say $\eta = 0.5$ the motion becomes regular as shown in Fig. 12(c). The transition between regular and chaotic motions is represented in Fig. 12(c). In that picture a new periodic attractor appears (its basin is plotted in white color) as we suggest in the bifurcation diagrams.

5. Conclusions and Discussion

Our results show that the nonsmooth systems can be studied by the Melnikov criterion. Here, we propose to rely on the numerical integration of the Melnikov integral. The advantage of our method is to use a single formula to obtain the critical value of the force-to-damping ratio. Furthermore, we investigated the difference caused by the additional spring which is useful in problems related to suspension of vehicles. We observed it in both analytical critical curve and also in the series of pictures showing both the bifurcation diagrams and the basins of

attraction evolution. In the analytical part we have shown the different regions of parameters F , α and ω in which the dynamics is periodic or chaotic.

The numerical bifurcation diagrams elucidate clearly the role of F , k and ω for which the onset of the chaotic motions takes place. Besides, by analyzing the different numerical bifurcation diagrams we conjecture both, the appearance and destruction of different attractors. This last result is corroborated by analyzing the evolution of the basin of attraction for different values of η . The basins of attraction show us, for values of η close to the critical points in which the dynamics changes from periodic to chaotic or vice versa, these creations and destructions of the different attractors for which both the numerical and the theoretical results are in complete agreement.

Finally, these results encourage us to apply the above approach to other systems with nonsmoothness including the clearance and dry friction phenomena which have important and relevant implications in engineering [Wiercigroch & de Kraker, 2000; Radons & Neugebauer, 2004].

Acknowledgments

We would like to thank Juan C. Vallejo for the fruitful discussions we had during the development of this work. The basins of attraction (Figs. 11 and 12) have been created using the software DYNAMICS [Nusse & Yorke, 1997]. This work was supported by the Spanish Ministry of Science and Innovation under project number FIS2009-09898. J. Seoane

acknowledges the warm hospitality received at Lublin University of Technology where part of this work was carried out. This paper has been partially supported by the 7th Framework Programme, contract No. FP-7 245479. M. A. F. Sanjuán acknowledges the hospitality of the Beijing Jiaotong University under the “Key Invitation Program for Top-Level Experts” of the “State Administration of Foreign Experts Affairs” of China.

References

- Aguirre, J. & Sanjuán, M. A. F. [2002] “Unpredictable behavior in the Duffing oscillator: Wada basins,” *Physica D* **171**, 41–51.
- Aguirre, J., Viana, R. L. & Sanjuán, M. A. F. [2009] “Fractal structures in nonlinear dynamics,” *Rev. Mod. Phys.* **81**, 333–386.
- Almendral, J. A., Seoane, J. M. & Sanjuán, M. A. F. [2004] “Nonlinear dynamics of the Helmholtz oscillator,” *Recent Res. Dev. Sound Vib.* **2**, 115–150.
- Baltanás, J. P., Trueba, J. L. & Sanjuán, M. A. F. [2001] “Energy dissipation in a nonlinearly damped Duffing oscillator,” *Physica D* **159**, 22–34.
- Baltanás, J. P., Trueba, J. L. & Sanjuán, M. A. F. [2002] “Nonlinearly damped oscillators,” *Recent Res. Dev. Sound Vib.* **1**, 29–61.
- Burden, R. L. & Faires, J. D. [1997] *Numerical Analysis* (ITP, USA).
- Duffing, G. [1918] *Erzwungene Schwingungen bei Veränderlicher Eigenfrequenz* (F. Vieweg u. Sohn, Braunschweig).
- Guckenheimer, J. & Holmes, P. J. [1983] *Nonlinear Oscillations, Dynamical Systems and Bifurcations of Vectorfields* (Springer, NY).
- Holmes, P. J. [1979] “A nonlinear oscillator with a strange attractor,” *Philos. Trans. Roy. Soc. London A* **292**, 419–448.
- Kunze, M. & Küpper, T. [2001] “Nonsmooth dynamical systems: An overview,” in *Ergodic Theory, Analysis, and Efficient Simulation of Dynamical Systems*, ed. Fiedler, B. (Springer, Berlin-NY), pp. 431–452.
- Leine, R. I., van Campen, D. H. & van de Vrande, B. L. [2000] “Bifurcations in nonlinear discontinuous systems,” *Nonlin. Dyn.* **23**, 105–164.
- Litak, G., Borowiec, M. & Syta, A. [2007] “Vibration of generalized double well oscillators,” *Zeit. Angew. Math. Mech.* **87**, 590–602.
- Litak, G., Borowiec, M., Friswell, M. I. & Szabelski, K. [2008] “Chaotic vibration of a quarter-car model excited by the road surface profile,” *Comm. Nonlin. Scien. Numer. Simul.* **13**, 1373–1383.
- Melnikov, V. K. [1963] “On the stability of the center for time periodic perturbations,” *Trans. Mosc. Math. Soc.* **12**, 1–57.
- Moon, F. C. & Li, G. X. [1985] “Fractal basin boundaries and homoclinic orbits for periodic motion in a two-well potential,” *Phys. Rev. Lett.* **55**, 1439–1443.
- Nusse, H. C. & Yorke, J. A. [1997] *Dynamics: Numerical Explorations* (Springer, NY, USA).
- Pavlovskaja, E. & Wiercigroch, M. [2007] “Low-dimensional maps for piecewise smooth oscillators,” *J. Sound Vib.* **305**, 750–771.
- Radons, G. & Neugebauer, R. [2004] *Nonlinear Dynamic Effects of Production Systems* (Wiley-VCH, Weinheim).
- Robinson, R. C. [2004] *Dynamical Systems: Continuous and Discrete* (Prentice Hall, London, UK).
- Sprott, J. C. [2003] *Chaos and Time Series Analysis* (Oxford University Press, NY).
- Verros, G., Natsiavas, S. & Stepan, G. [2000] “Control and dynamics of quarter-car models with dual-rate damping,” *J. Vib. Contr.* **6**, 1045–1063.
- Von Wagner, U. [2004] “On non-linear stochastic dynamics of quarter car models,” *Int. J. Non-Linear Mech.* **39**, 753–765.
- Wiercigroch, M. & de Kraker, B. [2000] *Applied Nonlinear Dynamics and Chaos of Mechanical Systems with Discontinuities*, Word Scientific Series on Nonlinear Science A, Vol. 28 (World Scientific, Singapore).